# The disruption of CtBP regulates DUX-dependent and -independent genetic program for the 2-cell-like state in murine embryonic stem cells

Kota Sugiyama[1], Kazuma Yoshioka[1], Nao Hayakawa[1], Miyu Marutani, Ryo Masuda, Selma Alamanda Abadi, Maki Ichisakino and Yoshiyuki Seki

Department of Biomedical Sciences, School of Biological and Environmental Sciences, Kwansei Gakuin University, Hyogo, Japan

[1]Co-first author

[*]Correspondence: yseki@kwansei.ac.jp

**Abstract**

After fertilization, maternally deposited mRNA is cleared, and *de novo* mRNA is transcribed from the zygotic genome through zygotic genome activation (ZGA), which is called maternal-to-zygotic transition (MZT) occurring in the mouse at 2-cell (2C) stage. 2C-like cells (2CLCs) marked by MERVL expression and transcriptionally similar to 2C embryos spontaneously emerge from mouse embryonic stem cells (mESCs). Although the emergence of 2CLCs completely depends on DUX function, a recent knockout study clearly showed that DUX is dispensable for mouse embryos, suggesting that DUX-independent molecular pathways are not recapitulated in 2CLCs. We present here that the disruption of C-terminal binding protein 1/2 (*Ctbp1/2*) activates DUX-dependent and -independent molecular pathway associated with the development of early mouse embryos mediated by the upregulation of Preferentially expressed antigen of melanoma family-like 7 (PRAMEL7). Furthermore, the abnormality of the gene expression profile caused by *Dux* KO is partially rescued by the overexpression of PRAMEL7 in mESCs. Our study provides new insights into the DUX-independent molecular pathway for developing early mouse embryos.

## Introduction

After fertilization, maternal factors direct development and trigger zygotic genome activation (ZGA) at the around late one-cell stage in mice, called maternal-to-zygotic transition (MZT)(Eckersley-Maslin et al., 2018). The early-cleavage stage embryos acquire cellular totipotency to generate both embryonic proper and extraembryonic tissues during MZT. Although totipotency was thought to be exclusive to the early-cleavage stage embryos, a part of the molecular network is recapitulated in the totipotent-like cells (2-cell-like cells; 2CLCs) marked by the expression of endogenous retrovirus MERVL, which are an endogenous subpopulation of mouse embryonic stem cells (ESCs). (Macfarlan et al., 2012a) (Rodriguez-Terrones et al., 2018).

The transition from pluripotent stem cells into 2CLCs is a useful *in vitro* system for identifying the gene regulatory network for ZGA, and several genes that control the emergence of 2CLCs from pluripotent cells have been identified (Eckersley-Maslin et al., 2019; Hu et al., 2020; Ishiuchi et al., 2015; Percharde et al., 2018; Rodriguez-Terrones et al., 2018). The transcription factor DUX (DUX4 in humans) is a critical factor for regulating the transition from pluripotent stem cells into 2CLCs and the expression of ZGA genes (De Iaco et al., 2017; Hendrickson et al., 2017; Whiddon et al., 2017). Ectopic expression of DUX enhances the population of 2CLCs, whereas the *Dux* disruption eliminates the emergence of spontaneous 2CLCs during mESC culture. Several 2CLC regulatory genes have been identified, but they are either direct activators (DPPA2/4, p53 and NELFA) or direct repressors (CAF-1, LINE-1 and SETDB1) of *Dux* expression (Eckersley-Maslin et al., 2019; Grow et al., 2021; Ishiuchi et al., 2015b; Percharde et al.,

2018; Wu et al., 2020). However, both *Dux* zygotic and maternal knockout embryos can survive full-term (Chen and Zhang, 2019; Guo et al., 2019), suggesting that DUX-independent molecular pathways not recapitulated in 2CLCs are critical for ZGA and the early development of mice.

In this study, we show that disruption of Ctbp1/2 (C-terminal binding protein 1/2) (Stankiewicz et al., 2014) activates two distinct sets of genes in ESCs: the first set is transiently upregulated in a DUX-dependent manner during minor ZGA, and the second set contains maternally expressed genes and the upregulated genes in a DUX-independent manner during major ZGA. Preferentially Expressed Antigen in Melanoma (PRAME) 7 is directly upregulated by the loss of *Ctbp1/2* without DUX function, and upregulated PRAMEL7 activates minor ZGA genes in a DUX-dependent manner and maternally expressed genes and major ZGA in DUX-independent manner. These data revealed that the disruption of *Ctbp1/2* recapitulates a part of DUX-independent ZGA cascades in ESCs, and *Ctbp1/2* DKO ESCs are useful *in vitro* systems to investigate DUX-independent molecular cascades ensuring ZGA in mice.

71 **Material and Methods**

72 **Cell Culture**

73 E14tg2a ESCs (RIKEN Cell Bank) were cultured in Glasgow minimum essential medium
74 (GMEM; Wako) containing 10% fetal calf serum (FCS; Invitrogen), 1 mM glutamine
75 (Wako), nonessential amino acids (Wako) and 500 μM Monothioglycerol Solution
76 (Wako). The culture was supplemented with 1000 U/ml of leukaemia inhibitory factor
77 (LIF) (Wako) without feeder cells. ESCs were cultured in N2B27 medium with 2i
78 (PD0325901, 0.4 μM: WAKO, CHIR99021, 3 μM: Sigma-Aldrich).

79

80 **Generation of knockout ESCs using a CRISPR-Cas9 system**

81 Guide RNAs for *Ctbp1/2*, *Dux* and *Pramel7* were generated in pX330-U6- Chimeric_BB-
82 CBh-hSpCas9 (Addgene plasmid #42230; deposited by Feng Zhang; Cong et al., 2013).
83 The guide RNA sequences are listed in Supplementary Table 1. The pX330 was co-
84 transfected with pCAG-EGFP into E14tg2a with MERVL::TurboGFP (Addgene plasmid
85 #69072; deposited by Maria-Elena Torres-Padilla; (Ishiuchi et al., 2015a). The GFP-
86 positive fraction was sorted by Cell Sorter (No. SH800; Sony Biotechnology, Inc., Tokyo,
87 Japan). Genomic DNA deletions were sequenced (Supplementary Figure 1).

88

89 **qRT-PCR and RNA-Seq**

90 Total mRNA was purified with a PureLink$^{TM}$ RNA Mini Kit (Ambion, Inc.). For
91 quantitative RT-PCR, cDNA was synthesized by ReverTra Ace® qPCR RT master Mix
92 (Toyobo), and then analyzed by qPCR with FastStart SYBR Green Master Mix (Roche)

93 using a specific primer set for each gene (Supplementary Table 1). RNA-seq libraries
94 were generated using Collibri™ Stranded RNA library prep for illumina™ Systems
95 (ThermoFisher Scientific) and sequenced using HiSeq X™ Ten (Illumina) (150-bp
96 paired-ends reads).
97
98 **Data analysis of RNA-Seq**
99 Total mRNA was purified with a PureLink™ RNA Mini Kit (Ambion, Inc.). RNA-seq
100 libraries were generated using Collibri™ Stranded RNA library prep for illumina™
101 Systems (ThermoFisher Scientific) and sequenced using HiSeq X™ Ten (Illumina).
102 Reads were aligned by Hisat2 to the Mus musculus genome (mm10). Raw read counts of
103 genes were calculated by R package FeatureCounts using mm10 KnownGenes. GTF from
104 UCSC for annotation. Normalized count data, principal component and K-means
105 clustering analysis were exported by the interactive Expression and Pathway analysis
106 (iDEP) webserver using the count data or normalized expression data of early mouse
107 embryos (Ge et al., 2018). Gene set enrichment analysis (GSEA) was used to determine
108 whether upregulated genes by *Ctbp1/2* knockouts were enriched for the upregulated genes
109 in 2-cell embryos or 2CLCs as described previously. Venn diagrams showing overlapping
110 genes were constructed by BioVenn, a web application (Hulsen et al., 2008).
111
112 **Bisulfite sequencing of specific genes and RRBS**
113 Genomic DNA was purified using Wizard® SV Genomic DNA Purification System
114 (Promega). For bisulfite sequencing of specific genes, the unmethylated cytosine of the

115 genomic DNA was converted to uracil using EpiTect Bisulfite Kit (QIAGEN) according
116 to the manufacturer's instructions. Bisulfited DNA was amplified by the region-specific
117 primer, followed by the sequencing. According to the manufacturer's instructions, DNA
118 libraries for RRBS analysis were prepared using the Premium RRBS kit V2 and
119 sequenced using HiSeq X$^{TM}$ Ten (Illumina) (150-bp paired-ends reads). RRBS reads
120 were trimmed using trim galore (www.bioinformatics.babraham.ac.uk/projects/
121 trim_galore/) with the RRBS option invoked. Bismark was used to align reads to UCSC
122 version mm10 of the mouse genome. CpG methylation was extracted using
123 bismark_methylation_extractor and displayed by Broad Institute's Integrative Genomic
124 Viewer (IGV) (Robinson et al., 2011).
125
126 **Immunofluorescence analysis**
127 Cells were fixed by 4% paraformaldehyde at 4°C for 20 min, followed by incubation with
128 PBS containing 0.5% Triton-X at 4°C for 5 min. Permeabilized cells were incubated with
129 a primary antibody solution containing anti-GFP (Nacarai Tesque, 04404-84, 1:500) with
130 anti-ZSCAN4 (Merk Millipore, AB4340, 1:1000) or anti-MuERVL-Gag (Epigentek, A-
131 2801-050, 1:250) or anti-OCT4 (Santa Cruz, Sc-8628, 1:500) or anti-CtBP2 (BE
132 Biosciences, 612044, 1:500) followed by secondary antibody solution containing anti-
133 Rat IgG Dylight$^{TM}$ 488 antibody (Rockland, 612-141-120, 1:500) or anti-Rabbit IgG
134 Dylight$^{TM}$ 549 antibody (KPL, 042-04-15-06, 1:500) or anti-Mouse IgG Dylight® 550
135 antibody (Abcam, ab96876, 1:500) or anti-Goat IgG Dylight$^{TM}$ 549 antibody (Rockland,
136 605-742-002, 1:500) with 1 μg/ml of DAPI solution (DOJINDO, 340-07971).

137

138 **Luciferase assay**

139 The enhancer candidate region of *Pramel7* or *Dux* was cloned into pGL4.23, driving the
140 *luciferase* gene. Wild-type or *Ctbp1/2* DKO ESCs were transfected with the reported
141 constructs with *Ctbp2* or *Pramel7* expression vector using HilyMax (DOJINDO). Cells
142 were harvested 36 hours after transfection, and the luciferase activities were measured
143 using the Dual-luciferase Reporter Assay System (Promega).

144

145 **Western blotting analysis**

146 Cells were lysed by boiling SDS sample buffer (WAKO). Before lysed proteins were
147 applied to polyacrylamide-SDS gels, 2-mercaptoethanol was added to denature the
148 proteins. The lysed proteins were separated on polyacrylamide-SDS gels, blotted on a
149 polyvinylidene fluoride membrane, and probed using the following primary antibodies:
150 anti-UHRF1 (MBL, D289-3, 1:1000) or anti-TUBLIN (SIGMA, T5168, 1:5000).
151 Following the primary antibody reaction, the membrane were incubated with horseradish
152 peroxidase (HRP)-coupled secondary antibodies. All antibodies were detected with
153 Immunostar LD (WAKO).

154

155 **Phylogenetic tree inference**

156 Amino acid sequences of PRAME family proteins were obtained from Ensemble release
157 112. Multiple-sequence alignment was performed using the ClustalW algorithm with the

158 MEGA software, version 11 with default parameters. Molecular phylogenetic trees were

159 inferred with the maximum-likelihood method using MEGA software, version 11 with

160 default parameters.

161

162

163

164

165

166 **Results**

167 ***Ctbp1/2 Deficiency enhances the transition from pluripotent stem cells to 2-cell-like***
168 ***Cells***

169 We have previously shown that the CtBP1/2 are required to transition from formative to
170 naïve pluripotency in mouse embryonic stem cells (mESCs) (Yamamoto et al., 2020). To
171 elucidate the molecular functions of CtBP1/2 in the transition from formative to naïve
172 pluripotency in mESCs, we compared the gene expression profile between wild-type
173 (WT) and *Ctbp1/2* double knockout (DKO) ESCs using RNA-sequencing (RNA-Seq).
174 MA-plot comparing WT ESCs with *Ctbp1/2* DKO ESCs showed that the 2-cell (2C)-
175 restricted genes, including *Dux*, *Zscan4* and *Zfp352*, as well as three repeat elements
176 MERVL, MT2 and GSAT_Mm are significantly upregulated by *Ctbp1/2* DKO (Figure
177 1A, B). Gene set enrichment analysis (GSEA) using a 2-cell embryo and 2-cell-like cell
178 (2CLC)-enriched genes (404) (Macfarlan et al., 2012) showed that 2C-restricted genes
179 were significantly enriched in the upregulated genes by the loss of *Ctbp1/*2 (Figure 1C).
180 Next, to monitor the dynamics of the transition from pluripotent stem cells into 2C-like
181 cells, we established *Ctbp1/2* DKO ESCs carrying the turboGFP reporter under the
182 control of MERVL long terminal repeat (*Mervl*-EGFP) (Ishiuchi et al., 2015a). The GFP-
183 positive fraction was about 0.1 % in WT ESCs, while remarkedly, *Ctbp1/2* DKO induced
184 a more than 50-fold increase of 2CLC (7.37%). To confirm the critical markers of 2CLCs,
185 we performed immunofluorescence analysis with anti-ZSCAN4, Mervl-GAG and OCT4
186 antibodies (Figure 1E). *Mervl*-EGFP-positive cells emerged by *Ctbp1/2* DKO expressed
187 ZSCAN4 and Mervl-GAG and lacked OCT4. Our data suggested that the downregulation

188 of *Ctbp1/2* might be involved in the zygotic genome activation *in vivo*. Consistent with
189 this idea, maternal mRNA of CtBP2 was reduced between the 2-cell to 4-cell stage based
190 on the single-cell RNA-Seq data of mouse early embryo (Gerlinger et al., 2014) (Figure
191 1F). However, the expression level of CtBP2 was maintained in spontaneous 2CLCs
192 (Figure 1G), suggesting that the molecular pathway triggered by the loss of *Ctbp1/2* in
193 the 2-cell embryo is stalled in spontaneous 2CLCs.

194 **Figure 1**

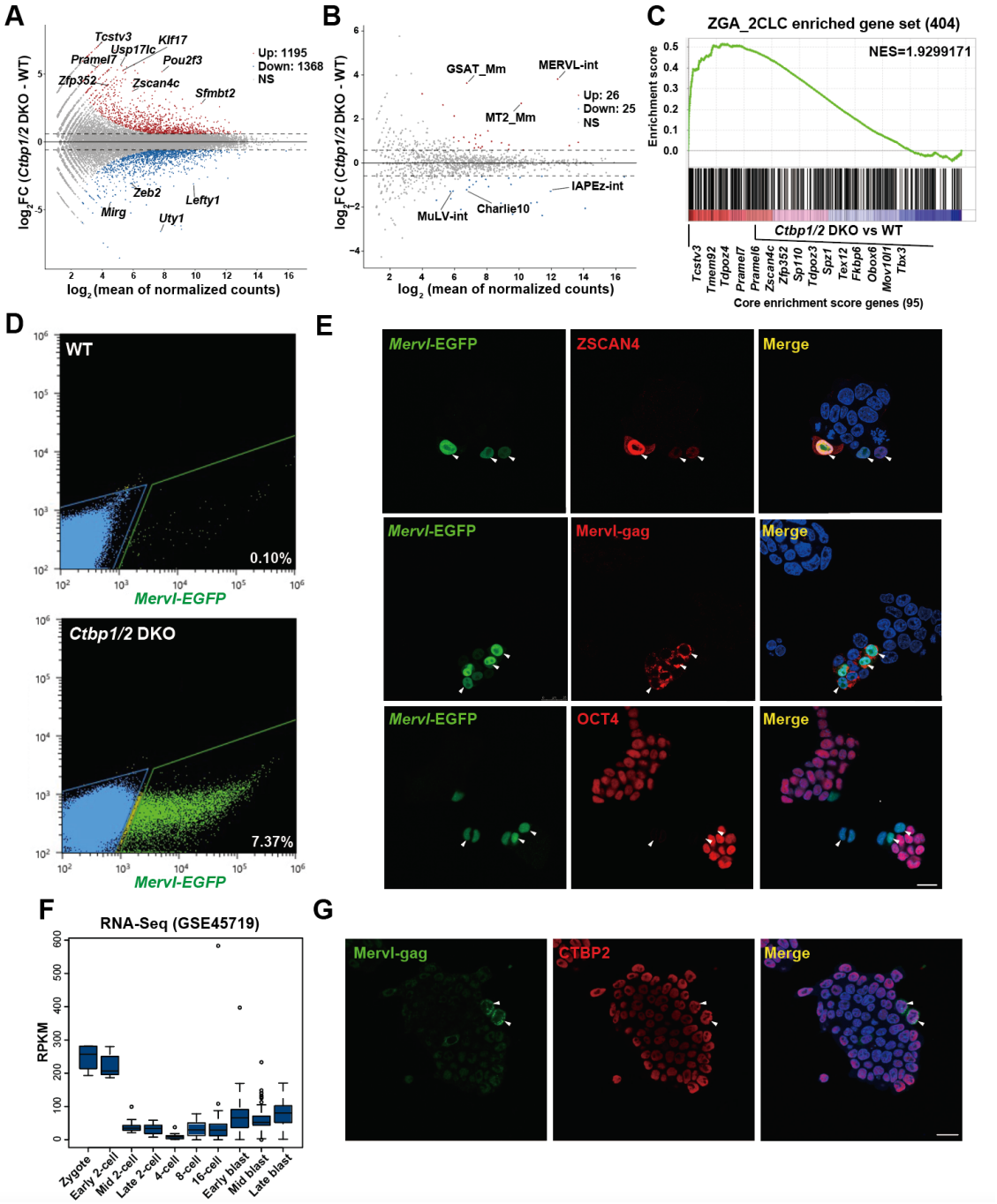


195 **Figure 1. The disruption of *Ctbp1/2* expands the 2-cell-like cells**

196 (A), (B) MA-plot showing mean expression and fold change per gene or repeat elements
197 in *Ctbp1/2* DKO versus WT ESCs. Cut-off values were set to 0.05 ≥ *P* and over 2-fold
198 changes. Red and blue dots indicate upregulated genes and downregulated genes,
199 respectively. (C) Gene set enrichment analysis (GSEA) using ZGA and 2-cell enriched
200 genes defined in (GSE33923) (Macfarlan et al., 2012)to compare *Ctbp1/2* DKO ESCs

201 with WT ESCs. (D) FACS analysis of MERVL::TurboGFP in WT ESCs and *Ctbp1/2*
202 DKO ESCs. (E) MERVL::TurboGFP-positive cells were marked by ZSCAN4 and Mervl-
203 gag proteins and mutually exclusive with OCT4-positive cells. Scale bar: 10 μm. (F)
204 mRNA levels of *Ctbp2* in early mouse development based on the published single-cell
205 RNA-Seq data (Gerlinger et al., 2014). (G) Immunofluorescence for CtBP2 (red) in WT
206 ESCs with MERVL::TurboGFP (green). Scale bar: 10 μm.
207

208 ***2C program induced by Ctbp1/2 Deficiency partially depends on DUX***

209 DUX, the homeobox transcription factor, is essential and sufficient for the emergence of
210 spontaneous 2CLCs from ESCs (De Iaco et al., 2017; Whiddon et al., 2017). To determine
211 the dependency of the 2C program driven by *Ctbp1/2* deficiency on DUX, we deleted the
212 *Dux* cluster in WT and *Ctbp1/2* DKO ESCs (Supplementary Figure 1C). Firstly, we
213 compared the population of MERVL-EGFP-positive cells between *Ctbp1/2* DKO and
214 *Ctbp1/2*/*Dux* TKO ESCs. Although *Dux* KO lost most of the MERVL-EGFP-strong
215 positive cells in *Ctbp1/2* DKO ESCs, MERVL-EGFP-weak positive cells were found in
216 *Ctbp1/2*/*Dux* TKO ESCs (Figure 2A). We have analyzed the expression levels of 2C
217 genes in WT, *Dux* KO, *Ctbp1/2* DKO and TKO ESCs using qRT-PCR. Upregulation of
218 Preferentially Expressed Antigen in Melanoma-like 7 (*Pramel7*) (Graf et al., 2017),
219 which is upregulated at the 2C stage of the mouse embryo (Guo et al., 2019), by the loss
220 of *Ctbp1/2* was unaffected by *Dux* KO, while *Dux* KO downregulated the expression of
221 *Zscan4c* in *Ctbp1/2* DKO ESCs (Figure 2B). Next, to determine the effect of the loss of
222 *Ctbp1/2* and *Dux* in the transcriptional activity of MERVL-LTR, we performed a
223 luciferase assay using the reporter driven by MERVL-LTR. *Ctbp1/2* deficiency
224 significantly upregulated the reporter driven by MERVL-LTR, and the mutation of the

225 DUX-recognition sequence impaired this activation, but the activity was substantially
226 higher than those in WT ESCs (Supplementary Figure 2A). Furthermore, the activation
227 of MERVL-Luciferase (Luc) by the loss of *Ctbp1/2* was significantly suppressed by the
228 deletion of *Dux*. However, the reporter activity of MERVL-Luc and MERVL-Luc with
229 the mutation of the DUX-recognition sequence (DUXm) in *Ctbp1/2*/*Dux* TKO ESCs was
230 considerably higher than those in *Dux* KO ESCs. These findings suggest that the loss of
231 *Ctbp1/2* activates the reporter activity of MERVL-Luc without the DUX function. qRT-
232 PCR analysis showed that the activation of *Zscan4c* is more strongly dependent on DUX
233 than the activation of *Mervl* and *Naalad2* by the loss of *Ctbp1/2* (Figure 2B). Published
234 ChIP-Seq data (Hendrickson et al., 2017) of DUX showed that DUX is localized at two
235 distinct regions around the *Zscan4c* locus (Supplementary Figure 2B). No MERVL
236 sequence was found at the major peak of DUX-binding, and the weak peak of DUX-
237 binding was localized in the MERVL sequence. In contrast, all DUX-binding peaks
238 around the *Naalad2* locus are co-localized with the MERVL sequence. These findings
239 suggested that *Zscan4c* is regulated by the DUX-binding elements with or without
240 MERVL, while only DUX-binding elements with MERVL regulate *Naalad2*. To confirm
241 these possibilities, we examined the reporter activity driven by DUX-binding elements
242 without MERVL and with MERVL. Reporter activity driven by the DUX-binding element
243 without MERVL upstream of *Zscan4c* was upregulated by the loss of *Ctbp1/2*, and this
244 activation was cancelled entirely by the deletion of *Dux* (Supplementary Figure 2C). The
245 reporter activity driven by the DUX-binding element with MERVL at *Zscan4c* and
246 *Naalad2* was also upregulated by the *Ctbp1/2* disruption, and this upregulation was

247 significantly but not entirely repressed by the loss of *Dux*. Consistent with the results of
248 MERVL-Luc, these reporter activities in *Ctbp1/2*/*Dux* TKO ESCs were higher than those
249 in *Dux* KO ESCs.
250 Next, to identify the 2C genes whose expression is upregulated by *Ctbp1/2* DKO without
251 DUX function, we performed RNA-Seq using WT, *Dux* KO, *Dppa2* KO, *Ctbp1/2* DKO,
252 *Ctbp1/2*/*Dux* TKO and *Ctbp1/2*/*Dppa2* TKO ESCs. DPPA2/DPPA4 complex is the
253 upstream element for the activation of *Dux* in ESCs (Eckersley-Maslin et al., 2019). To
254 gain insight into the dependency of DUX on the expression variation by the loss of
255 *Ctbp1/2*, we created a scatter plot displaying the correlation of expression variation by
256 the *Ctbp1/2* DKO between WT and *Dux* KO ESCs (Figure 2C). The distribution of the
257 scatter plots showed that the dependency of DUX on the transcriptional regulation by
258 *Ctbp1/2* is relatively weak, except for some genes, including *Zscan4*, *Sp110* and *Usp17*.
259 The minimal effect of DUX on CtBP1/2-mediated transcriptional regulation was
260 confirmed by gene set enrichment analysis (GSEA) comparing *Ctbp1/2/Dux* TKO and
261 *Dux* KO ESCs using the upregulated genes in *Ctbp1/2* DKO (Figure 2D).
262 We then performed K-means clustering analysis (K=5) using the top 2000 differentially
263 expressed genes to separate groups based on the expression alteration at each KO
264 condition (Figure 2E). DUX and DPPA2-dependent upregulated genes by the loss of
265 *Ctbp1/2,* including *Zscan4* and *Pramef25* (*Pramel16*), were enriched in Cluster 2. Cluster
266 3, which was enriched with a group of genes whose expression is reduced by *Dux* KO
267 and this reduction is canceled by *Ctbp1/2* DKO, contained KRAB-ZFP cluster
268 (*Zfp900*/*981*/*600*/*534*/*458*) (Wolf et al., 2020). Cluster 4, in which the genes are

269 upregulated by *Ctbp1/2* DKO, *Ctbp1/2/Dux* TKO and *Ctbp1/2/Dppa2* TKO, contained
270 the genes upregulated by major ZGA, including *Pramel6/7*, *Pramef17*, *Cphx1/2/3*, *Gata1*
271 and *Crxos* (Supplementary Table 2). Interestingly, Cluster 5, enriched with a group of
272 genes whose expression was decreased by *Dppa2* KO and increased by *Ctbp1/2* DKO,
273 was enriched in GO regarding reproduction, including *Tex11*, *Dazl* and *Hormad1*. To
274 verify whether the gene expression changes in ESCs induced by *Ctbp1/2* DKO reflect the
275 gene expression dynamics in early embryos, we analyzed the expression changes of genes
276 belonging to Cluster 2 (DUX-dependent genes), Cluster 4 (DUX-independent genes) and
277 Cluster 5 (DPPA2-dependent genes) in early mouse embryo using public RNA-Seq data
278 (Gerlinger et al., 2014) (Figure 2F and Figure 3A). We analyzed the expression dynamics
279 of Cluster 2 genes in early embryos by removing genes with low expression in early
280 embryos (FPKM $\leq$ 1). Most genes were transiently upregulated in 2-4 cell stages. In
281 contrast, K-means clustering (K=6) analysis of cluster 4 showed that they were classified
282 into two major groups: maternal factors whose expression decreased after fertilization
283 (Cluster4a and b) and genes whose expression was activated after ZGA (Cluster 4c-f).
284 Next, we focused on the loss of *Ctbp1/2, which* appears to reverse the gene expression
285 alteration caused by *Dux* KO, as shown in Clusters 3 and 4 of the K-means clustering
286 analysis. A comparison of the expression alteration by *Dux* KO in WT ESCs versus those
287 by the loss of *Ctbp1/2* in *Dux* KO ESCs, as demonstrated by scatter plots, revealed a
288 negative correlation (Figure 2G). Furthermore, the Venn diagram overlapping the
289 downregulated genes by *Dux* KO and the upregulated by *Ctbp1/2* DKO in *Dux* KO
290 showed that most of the down-regulated genes by *Dux* KO are upregulated by *Ctbp1/2*

291 DKO in *Dux* KO (Figure 2H). These results suggest that the loss of *Ctbp1/2* activates the

292 maternal genes and major ZGA genes located downstream of DUX, either directly or

293 indirectly.

294

**Figure 2**

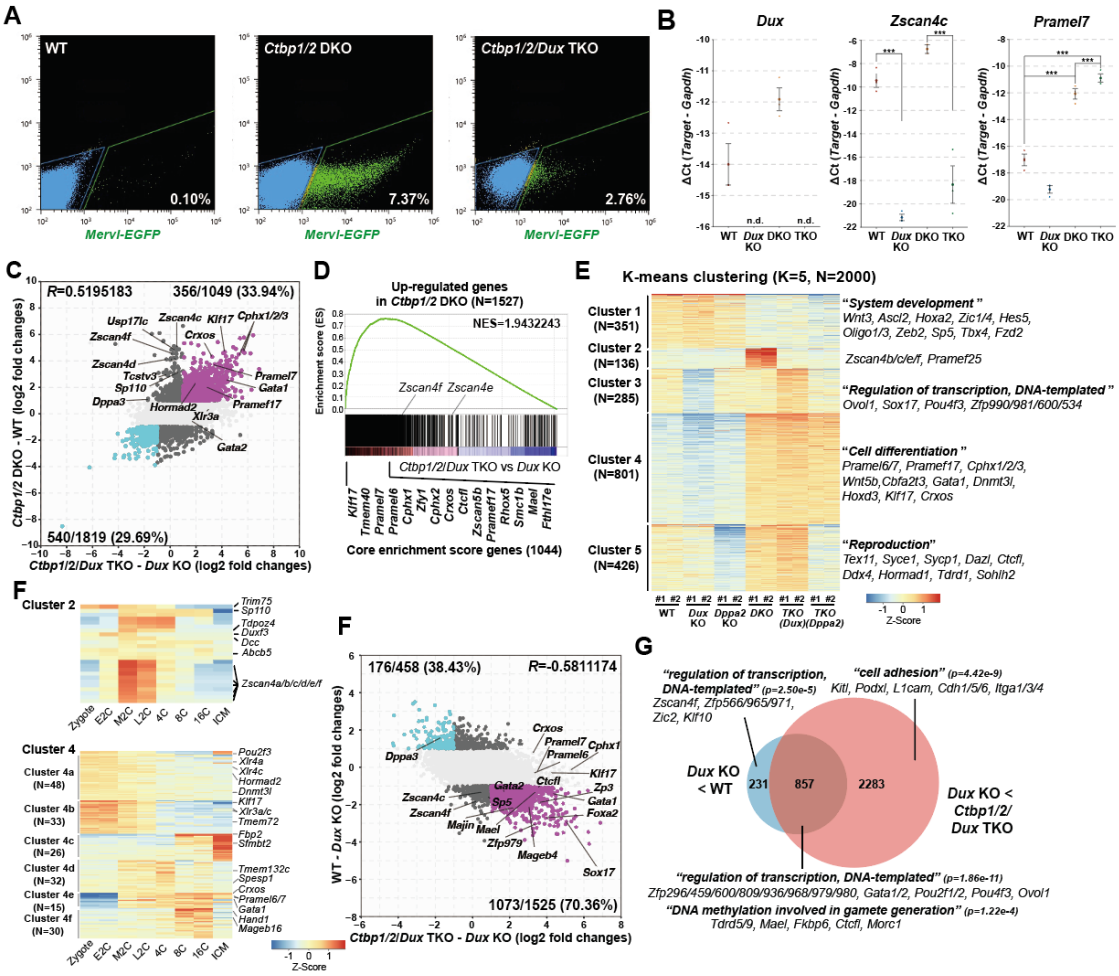


295

296 **Figure 2. *Ctbp1/2* disruption partially rescues the *Dux* KO phenotype in ESCs**

297 (A) FACS analysis of MERVL::TurboGFP in WT, *Ctbp1/2* DKO and *Ctbp1/2*/*Dux* TKO

298 ESCs. (B) RT-qPCR analysis of *Dux*, *Zscan4c* and *Pramel7* in WT, *Dux* KO, *Ctbp1/2*

299 DKO and Ctbp1/2/*Dux* TKO ESCs. The ΔCt of each gene was calculated by subtracting

300 the average Ct of each gene from that of *Gapdh*. Means of ΔCt were calculated from three

301 biological triplicates. ***$P < 0.001$, **$P < 0.005$, *$P < 0.05$ (Tukey-Kramer multiple

302 comparison test). (C) Scatter plot analysis of the correlation between the expression

303 changes by *Ctbp1/2* DKO in WT ESCs and *Ctbp1/2* DKO in *Dux* KO ESCs. (D) Gene
304 Set Enrichment Analysis (GSEA) of upregulated genes by *Ctbp1/2* DKO in *Ctbp1/2*/*Dux*
305 TKO and *Dux* KO ESCs. (E) Scatter plot analysis of the correlation between the
306 expression changes by *Dux* KO in WT ESCs and *Ctbp1/2* DKO in *Dux* KO ESCs. (F)
307 Gene Set Enrichment Analysis (GSEA) of the downregulated genes by *Dux* KO in
308 *Ctbp1/2*/*Dux* TKO and *Dux* KO ESCs. (G) K-means clustering analysis (K=5, N=2000)
309 using RNA-Seq data of WT, *Dux* KO, *Dppa2* KO, *Ctbp1/2* DKO, *Ctbp1/2*/*Dux* TKO and
310 *Ctbp1/2*/*Dppa2* TKO ESCs. K-means clustering analysis of the genes belonging to
311 Cluster 2 and Cluster 4 using published single-cell RNA-Seq data of early mouse embryos
312 (Gerlinger et al., 2014). (H) Venn diagram illustrating the overlap between the down-
313 regulated genes by *Dux* KO and the upregulated genes by *Ctbp1/2* DKO in *Dux* KO. (I)
314 Volcano plot showing differentially accumulated repetitive elements between WT ESCs
315 and *Dux* KO ESCs, WT ESCs and *Ctbp1/2* DKO ESCs, *Dux* KO ESCs and *Ctbp1/2*/*Dux*
316 TKO ESCs.
317

318 ***Dppa2 KO phenotype is partially rescued by the disruption of Ctbp1/2***

319 K-means clustering analysis of transcriptome data using WT, *Ctbp1/2* DKO, *Dppa2* KO
320 and *Ctbp1/2*/*Dppa2* TKO ESCs revealed that down-regulated genes by *Dppa2* KO tend
321 to be upregulated by *Ctbp1/2* DKO (Cluster 5) (Figure 2C). These genes were categorized
322 into two groups based on the gene expression dynamics in early embryos: maternally
323 expressed genes (Cluster 1, 2) and the genes activated after major ZGA (Cluster 3-5)
324 (Figure 3A). Comparing the expression changes caused by *Dppa2* KO in WT ESCs with
325 those caused by *Ctbp1/2* DKO in *Dppa2* KO ESCs showed a clear negative correlation
326 (Figure 3B). The Venn diagram illustrating the overlap between the genes downregulated
327 by *Dppa2* KO and those upregulated by *Ctbp1/2* DKO in *Dppa2* KO showed that
328 approximately half of the genes downregulated by *Dppa2* KO were upregulated by

329 *Ctbp1/2* DKO in *Dppa2* KO (Figure 3C). It was previously reported that DPPA2
330 safeguard against *de novo* DNA methylation through the establishment of H3K4me3
331 enrichment in ESCs cultured in 2i plus LIF condition (2iL) (Gretarsson and Hackett,
332 2020)(Eckersley-maslin et al., 2020). We compared the DNA methylation status at around
333 the CpG island of *Dazl* and promoter regions of LINE1 in WT, *Dppa2* KO, *Ctbp1/2* DKO,
334 *Ctbp1/2*/*Dppa2* TKO ESCs with serum LIF (SL) and 2iL using bisulfite sequencing
335 analysis. DNA methylation levels were consistently elevated by *Dppa2* KO in WT ESCs
336 but not in *Ctbp1/2* DKO, and this tendency was more pronounced in ESCs with 2iL than
337 SL (Figure 3D). We compared the global DNA methylation levels in WT, *Dppa2* KO,
338 *Ctbp1/2* DKO and *Ctbp1/2/Dppa2* TKO ESCs under 2iL using reduced-representation
339 bisulfite sequencing (RRBS). Because it has been reported that DPPA2 preferentially
340 binds to CpG island and protects aberrant *de novo* DNA methylation (Gretarsson and
341 Hackett, 2020), we extracted the promoter region with CpG island in which the DNA
342 methylation levels were elevated by *Dppa2* KO in ESCs (Figure 3E). Interestingly, the
343 DNA methylation levels at almost all these promoter regions, including meiosis-
344 associated genes, *Dazl*, *Ddx4* and *Sycp1/2/3*, were reduced by the disruption of *Ctbp1/2*
345 in *Dppa2* KO ESCs. (Figure 3E, F). To determine the molecular mechanism that *Ctbp1/2*
346 disruption impaired the abnormal elevation of DNA methylation caused by *Dppa2* KO in
347 ESCs, we compared the mRNA expression of the regulators of DNA methylation and
348 DNA methyltransferases by RT-qPCR analysis. *Pramel7,* which is involved in degrading
349 UHRF1 protein (Graf et al., 2017), was significantly repressed in *Dppa2* KO ESCs, and
350 this repression was entirely cancelled by *Ctbp1/2* disruption (Figure 3G). Consistent with

351 the expression of *Pramel7*, the protein level of UHRF1 was elevated by *Dppa2* KO, and
352 this up-regulation was diminished by *Ctbp1/2* disruption (Figure 3H). RRBS and
353 published ChIP-Seq data of DPPA2 (Engelen et al., 2015) showed that DNA methylation
354 level was elevated upstream region of *Pramel7* associated with DPPA2-binding (Figure
355 3I), suggesting that DPPA2 maintain DNA hypomethylation through the activation of
356 *Pramel7* expression.

357

# Figure 3

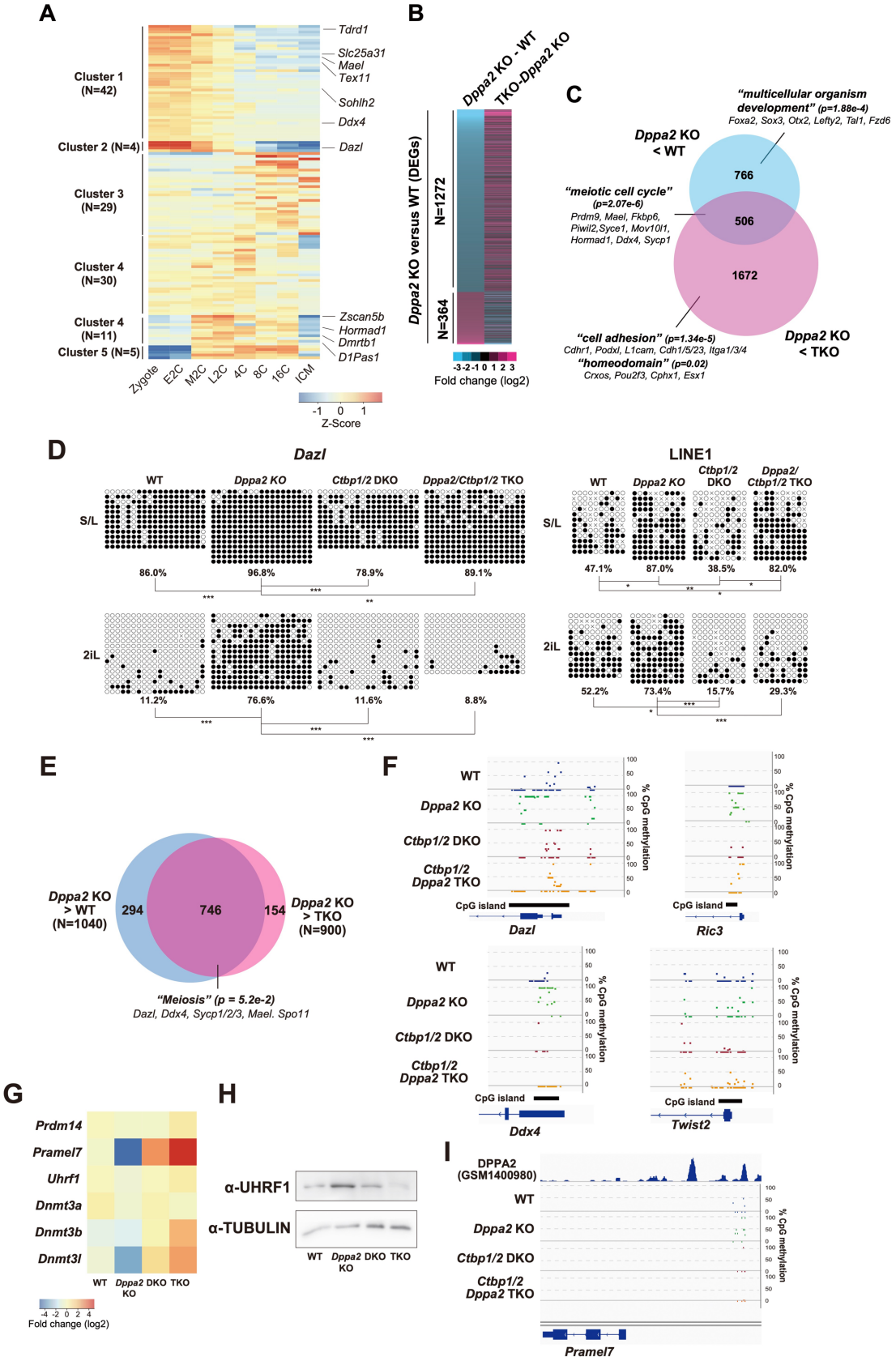
A
Cluster 1 (N=42)
Cluster 2 (N=4)
Cluster 3 (N=29)
Cluster 4 (N=30)
Cluster 4 (N=11)
Cluster 5 (N=5)
Tdrd1
Slc25a31
Mael
Tex11
Sohlh2
Ddx4
Dazl
Zscan5b
Hormad1
Dmrtb1
D1Pas1
Zygote
E2C
M2C
L2C
4C
8C
16C
ICM
-1 0 1
Z-Score
B
Dppa2 KO - WT
TKO-Dppa2 KO
Dppa2 KO versus WT (DEGs)
N=1272
N=364
-3 -2 -1 0 1 2 3
Fold change (log2)
C
"multicellular organism development" (p=1.88e-4)
Foxa2, Sox3, Otx2, Lefty2, Tal1, Fzd6
Dppa2 KO < WT
766
"meiotic cell cycle" (p=2.07e-6)
Prdm9, Mael, Fkbp6, Piwil2,Syce1, Mov10l1, Hormad1, Ddx4, Sycp1
506
1672
"cell adhesion" (p=1.34e-5)
Cdhr1, Podxl, L1cam, Cdh1/5/23, Itga1/3/4
"homeodomain" (p=0.02)
Crxos, Pou2f3, Cphx1, Esx1
Dppa2 KO < TKO
D
Dazl
LINE1
WT
Dppa2 KO
Ctbp1/2 DKO
Dppa2/Ctbp1/2 TKO
S/L
2iL
86.0%
96.8%
78.9%
89.1%
11.2%
76.6%
11.6%
8.8%
47.1%
87.0%
38.5%
82.0%
52.2%
73.4%
15.7%
29.3%
E
Dppa2 KO > WT (N=1040)
294
746
154
Dppa2 KO > TKO (N=900)
"Meiosis" (p = 5.2e-2)
Dazl, Ddx4, Sycp1/2/3, Mael. Spo11
F
WT
Dppa2 KO
Ctbp1/2 DKO
Ctbp1/2 Dppa2 TKO
% CpG methylation
CpG island
Dazl
Ric3
Ddx4
Twist2
G
Prdm14
Pramel7
Uhrf1
Dnmt3a
Dnmt3b
Dnmt3l
WT
Dppa2 KO
DKO
TKO
-4 -2 0 2 4
Fold change (log2)
H
α-UHRF1
α-TUBULIN
WT
Dppa2 KO
DKO
TKO
I
DPPA2 (GSM1400980)
WT
Dppa2 KO
Ctbp1/2 DKO
Ctbp1/2 Dppa2 TKO
% CpG methylation
Pramel7

358 **Figure 3. The loss of *Ctbp1/2* rescues abnormal DNA methylation by *Dppa2* KO.**
359 (A) K-means clustering analysis of the genes of Cluster 5 (Figure 2C) using published
360 single-cell RNA-Seq data of early mouse embryos (Gerlinger et al., 2014). (B) A scatter
361 plot of RNA-Seq data represents genes upregulated or downregulated by *Dppa2* KO in
362 WT ESCs and *Ctbp1/2* DKO in *Dppa2* KO ESCs. (C) The Venn diagram shows the
363 overlapping between the down-regulated genes by *Dppa2* KO in WT ESCs and the
364 upregulated genes by *Ctbp1/2* DKO in *Dppa2* KO ESCs. (D) Bisulfite sequencing of the
365 promoter region of *Dazl* and *LINE1* in WT, *Dppa2* KO, *Ctbp1/2* DKO and
366 *Ctbp1/2*/*Dppa2* TKO ESCs under Serum LIF and 2i LIF. ***$P < 0.001$, **$P < 0.005$, *$P$
367 $< 0.05$ (Mann-Whitney U-test). (E) Venn diagram showing the overlapping between the
368 region with CpG island in which DNA methylation is elevated by *Dppa2* KO in ESCs
369 and the region with CpG island in which Ctbp1/2 DKO reduces DNA methylation in
370 *Dppa2* KO ESCs. (F) Gene track representing the methylation levels derived from RRBS
371 at *Dazl*, *Ddx4*, *Ric3* and *Twist2* in WT, *Dppa2* KO, *Ctbp1/2* DKO and *Ctbp1/2*/*Dppa2*
372 TKO ESCs under 2iL. (G) Heat map showing the qRT-PCR data of the regulators of DNA
373 methylation and DNA methyltransferases in WT, *Dppa2* KO, *Ctbp1/2* DKO and
374 *Ctbp1/2*/*Dppa2* TKO ESCs. (H) Western blotting of UHRF1 and TUBULIN in WT,
375 *Dppa2* KO, *Ctbp1/2* DKO and *Ctbp1/2*/*Dppa2* TKO ESCs. (I) Gene track representing
376 the DPPA2-binding peaks reconstructed using published data (Engelen et al., 2015) and
377 the methylation levels derived from RRBS upstream of *Pramel7* in WT, *Dppa2* KO,
378 *Ctbp1/2* DKO and *Ctbp1/2*/*Dppa2* TKO ESCs.

379

380 ***The loss of Ctbp1/2 controls two genetic cascades for ZGA: DUX-dependent and DUX-***
381 ***independent***

382 Next, to identify the direct target of CtBP1/2 controlling the emergence of MERVL-
383 EGFP-positive cells, we established *Ctbp1/2* DKO ESCs carrying the expression unit of
384 *Ctbp2* regulated by the doxycycline administration. We traced the expression dynamics
385 of some critical genes associated with zygotic genome activation (ZGA) using qRT-
386 PCR analysis. *Dux*, *Mervl*, *Zscan4c* and *Zfp352* were significantly decreased from 3 to 9

387 days after induction of *Ctbp2* in *Ctbp1/2* DKO ESCs, while these genes were
388 upregulated from 3 to 9 days (d12-d18) after the depletion of *Ctbp2* expression (Figure
389 4A). In contrast, *Pramel7* was sharply downregulated (d0-d3) or upregulated (d9-d12)
390 after *Ctbp2* induction or depletion in *Ctbp1/2* DKO ESCs. These findings suggested that
391 2-cell associated genes upregulated by the loss of *Ctbp1/2* are classified into two
392 categories: CtBP1/2-indirect target genes such as *Dux*, *Mervl*, *Zscan4c* and *Zfp352*, and
393 CtBP1/2-direct target genes such as *Pramel7*. To identify the direct and indirect targets
394 of CtBP2, we performed RNA-Seq using *Ctbp1/2* conditional KO (cKO) ESCs.
395 Principal component analysis (PCA) revealed that the global changes of gene
396 expression profiled by the short-term induction (d0-d3) or depletion (d9-d12) of *Ctbp2*
397 in *Ctbp1/2* DKO ESCs contributed PC1 axis in the opposite direction (Figure 4B). On
398 the other hand, the global gene expression changes profiled by the long-term induction
399 (d3-d9) or depletion of *Ctbp2* (d12-d18) in *Ctbp1/2* DKO ESCs contributed to the PC2
400 axis in the opposite direction. K-means clustering analysis revealed that CtBP2 rapidly
401 and positively regulated the genes associated with system development, including
402 *Ascl2*, *Zic1/4* and *Olig1/3* in ESCs (Figure 4C and Supplementary Table 1,2).
403 Interestingly, the downregulated genes by CtBP1/2 were separated into two groups. The
404 genes in cluster 2 containing minor ZGA genes, including *Dux*, *Zscan4*, *Zfp352* and
405 *Gm4340,* were repressed 3 to 9 days after *Ctbp2* induction (Figure 4C). Major ZGA
406 genes, including *Pramel6/7/14*, *Crxos* and *Gata1,* and maternal factors, including
407 *Pou2f3*, *Klf17* and *Pramef12* (*Pramel13*), were in cluster 3, in which the genes were
408 rapidly downregulated or upregulated by the loss or gain of *Ctbp2*. Next, to extract the

409 direct or indirect targets of CtBP2, we compared a group of genes rapidly or slowly
410 repressed by *Ctbp2* induction with a group of genes that are rapidly or delay activated
411 by *Ctbp2* depletion, respectively (Figure 4D, E). We defined overlapped genes as the
412 candidates for the direct target (rapid response genes) and indirect target of CtBP2
413 (delayed response genes), and we displayed the RNA-Seq data of parts of these genes in
414 the heatmap (Figure 4F). To determine the dependency of rapid response genes and
415 delayed response genes on DUX function, we constructed a Venn diagram illustrating
416 the overlap of DUX-independent upregulated genes with rapid response genes and
417 delayed response genes (Figure 4G). Almost all rapid response genes, but less than half
418 of delayed response genes, were upregulated by the loss of CtBP2 without DUX
419 function. Next, to identify the direct target of CtBP1/2, we overlapped the genes that
420 CtBP2 is localized within +/- 10 kb of the transcription start site (TSS) with rapid and
421 delayed response genes using the Venn diagram using public ChIP-seq data of CtBP2 in
422 ESCs (Kim et al., 2015) (Figure 4H). CtBP2 binding peaks were observed in
423 approximately half of the rapid response genes, whereas only two genes among the
424 delayed response genes exhibited CtBP2 binding peaks near their TSS. Next, we
425 displayed the ChIP-Seq track of DUX- and CtBP2-binding peaks and histone H3
426 Lysine-27 acetylation (H3K27Ac), a typical enhancer mark (Hendrickson et al., 2017)
427 (Kim et al., 2015)(Zhang et al., 2020), at around the *Pramel7*, *Pou2f3* (rapid response
428 genes) and *Duxf3*, *Zscan4*c (delayed response genes) (Figure 4I). CtBP2 was localized
429 within the H3K27Ac-enriched distal enhancer of *Pramel7* and *Pou2f3*. In contrast,
430 CtBP2-binding peaks were absent, and DUX-binding peaks were localized around the

431 TSS of *Duxf3* and *Zsacn4c*. To determine the direct effect of CtBP2 at the distal
432 enhancer of *Pramel7*, we analyzed the effect of CtBP2 overexpression against the
433 transcriptional activity driven by the distal enhancer of *Pramel7* in WT and *Ctbp1/2*
434 DKO ESCs (Figure 4J). Luciferase activity was activated in *Ctbp1/2* DKO ESCs
435 compared with those in WT ESCs, and the CtBP2 overexpression completely
436 diminished this activation. In summary, our findings indicate that the loss of CtBP1/2
437 controls two pathways regulating 2C programs: one mediated by *Dux* activation
438 (*Zscan4c* and *Usp17lc*) and the other directly activated by the loss of CtBP1/2 (*Prame7*
439 and *Pou2f3)*.

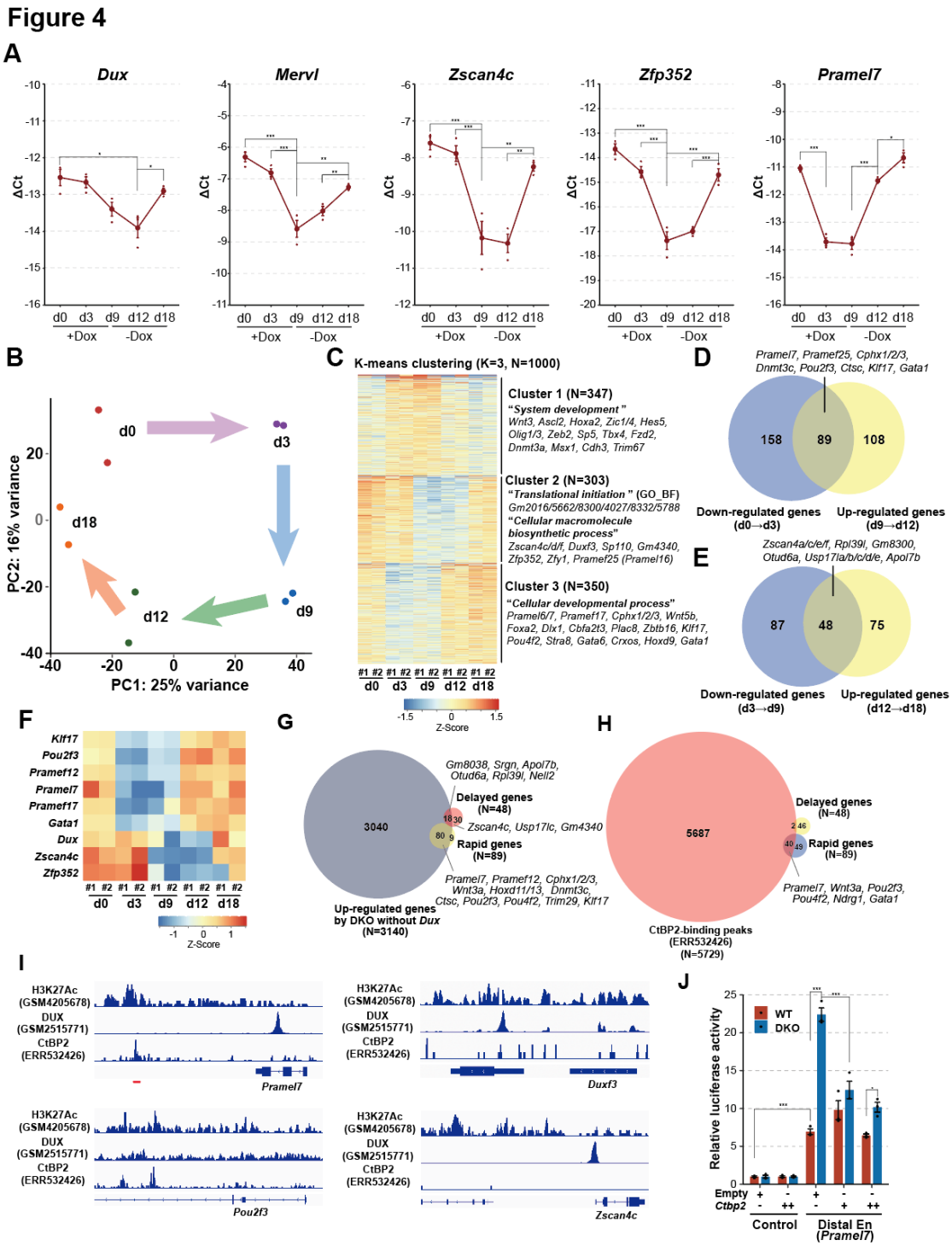


**Figure 4. The loss of *Ctbp1/2* controls two genetic cascades for ZGA.**

(A) RT-qPCR analysis of *Dux*, *Mervl, Zscan4c Zfp352* and *Pramel7* in *Ctbp1/2* DKO ESCs without Dox or with Dox. The ΔCt of each gene was calculated by subtracting the average Ct of Gapdh from that of each gene Ct. Means of ΔCt were calculated from

three biological triplicates. ***$P < 0.001$, **$P < 0.005$, *$P < 0.05$ (Tukey-Kramer multiple comparison test). (B) Principal component analysis (PCA) of *Ctbp1/2* DKO ESCs without Dox or with Dox. (C) K-means clustering analysis of *Ctbp1/2* DKO ESCs without Dox or with Dox using the top 1000 differentially expressed genes. (D) Venn diagram shows the overlapping of down-regulated genes three days after Ctbp2 induction and upregulated genes three days after *Ctbp2* removal. (E) Venn diagram showing the overlapping of down-regulated genes whose expression is down-regulated from 3 days to 9 days after *Ctbp2* induction and upregulated genes whose expression is upregulated from 3 days to 9 days after *Ctbp2* removal. (F) Heatmap showing the selected genes from K-means clustering analysis (C). (G) Venn diagram shows the overlapping of upregulated genes by *Ctbp1/2* DKO in *Dux* KO ESCs with rapid or gradual responses against *Ctbp2* expression. (H) The Venn diagram demonstrates the extent of overlap between CtBP2-binding genes and the rapid or gradual responses that are regulated by Ctbp2 expression. (I) Gene track of ChIP-Seq data of H3K27Ac (GSM4205678), DUX (GSM2525771) and CtBP2 (ERR532426) around *Pramel7*, *Pou2f3*, *Duxf3* and *Zscan4c*. The red bar indicates the region used for luciferase assay in (J). (J) The effect of CtBP2 overexpression for the enhancer activity of *Pramel7* distal enhancer (I) in *Ctbp1/2* DKO ESCs. Relative luciferase activity was calculated with the values of the empty vector as 1. Means of relative luciferase activity were calculated from three biological triplicates. ***$P < 0.001$, **$P < 0.005$, *$P < 0.05$ (Tukey-Kramer multiple comparison test).

***Prame family control genetic program of ZGA: DUX-dependent and -independent***

*Pramel7* belongs to the preferentially expressed antigen in melanoma (PRAME*)* gene family, which is restricted to the testis and various cancers (Kern et al., 2021). Because the PRAME family gene is one of the most amplified gene families in mammals and is considered the third largest gene family in the mouse genome (Church et al., 2009), we focused on the expression of the PRAME gene family in *Ctbp1/2* DKO ESCs. We collected the amino acid sequences of the PRAME family proteins annotated on the

474 mm10 genome sequence and created the phylogenetic tree (Supplementary Figures 3A).
475 The PRAME family genes were found to be clustered on six distinct chromosomes, and
476 a high similarity of PRAME family proteins was observed to occur on the same
477 chromosome (Supplementary Figure 3B). Next, we selected the expression levels of
478 PRAME family genes in WT, *Du*x KO, *Ctbp1/2* DKO and *Ctbp1/2/Dux* TKO from
479 RNA-Seq data and displayed the hierarchical clustering data in the heatmap (Figure
480 5A). Interestingly, most PRAME family genes, except for *Lrrc14*, *Lrrc14b*, and
481 *D5Ertd577e* (*Pramel48*), were upregulated in *Ctbp1/2* DKO ESCs. According to gene
482 expression patterns, the genes of the PRAME family can be grouped into four
483 categories. In the first category, including *Lrrc14*, there are genes whose expression is
484 unaffected by *Ctbp1/2* DKO. In the second category, including *Pramel6* and *Pramel14*,
485 the genes upregulated by *Ctbp1/2* DKO were further elevated by *Dux* KO. In the third
486 category, including *Pramel19* and *Pramel39*, the genes upregulated by *Ctbp1/2* DKO
487 were completely repressed by *Dux* KO (DUX-dependent PRAME family genes). In the
488 fourth category, including *Pramel7* and *Pramel12*, the genes upregulated by *Ctbp1/2*
489 DKO were unaffected by *Dux* KO (DUX-independent *Prame* family genes). Next, we
490 analyzed the expression dynamics of PRAME family genes in the early mouse embryo
491 using public scRNA-Seq data by removing genes with low expression in early embryos
492 (FPKM ≤ 1) (Gerlinger et al., 2014). *Pramel19* and *Pramel39*, DUX-dependent PRAME
493 family genes, were transiently upregulated at the mid-2-cell stage after transient
494 upregulation of *Dux* at the early 2-cell stage. DUX-independent PRAME family genes
495 were subdivided into three categories. The first category, including *Pramel6* and

496 *Pramel7*, adjacent to chromosome 2, were gradually upregulated from mid-2-cell to
497 peak expression at ICM. The genes, including *Pramel48* and *Pramel13* in the second
498 category, were not upregulated by ZGA. The genes belonging to the third category,
499 including *Pramel14* and *Pramel31,* were activated soon after ZGA and continued to be
500 expressed until 4 cell embryos. Because it has been reported that *Pramel7*, which is
501 upregulated by the loss of *Ctbp1/2* and ZGA not depending on DUX function, is critical
502 for early mouse development (Graf et al., 2017), we focused on the PRAMEL7
503 functions on the emergence of the 2CLCs from pluripotent stem cells. We generated
504 ESCs with forced expression of *Pramel7* with or without *Dux* KO (Figure 5C, D).
505 *Pramel7* overexpression expanded 2CLCs, and this expansion was entirely cancelled by
506 the *Dux* KO (Figure 5E, F). Gene set enrichment analysis comparing WT and *Pramel7*-
507 overexpressing ESCs using the upregulated genes by the loss of *Ctbp1/2* showed that
508 the upregulated genes by the loss of *Ctbp1/2* tended to be upregulated by *Pramel7*
509 overexpression (Figure 5G). Germline-specific genes and ZGA-associated genes were
510 consistently upregulated by the loss of *Ctbp1/2* and *Pramel7* overexpression (Figure
511 5H). Some sets of ZGA-associated genes, including *Crxos*, *Gata1* and *Klf17,* were only
512 upregulated by the loss of *Ctbp1/2*, suggesting that the loss of *Ctbp1/2* controls two
513 genetic cascades: PRAMEL7-dependent and PRAMEL7-independent pathway. Next,
514 we separated genes into five categories using K-means clustering analysis based on the
515 gene expression profiles in WT, *Dux* KO, *Pramel7*-OE and *Pramel7*-OE/*Dux* KO ESCs
516 (Figure 5I). The first category included the minor ZGA genes whose expression was
517 upregulated by PRAMEL7 depending on DUX functions. Most genes belonging to the

518 first cluster were transiently upregulated at mid-2-cell embryos soon after the transient
519 upregulation of *Dux,* such as the *Zscan4* family; the rest of the genes were upregulated
520 after eight-cell embryos (Figure 5J). *Dux* expression was elevated in PRAMEL7-
521 overexpressing ESCs (Figure 5K), and enhancer activity was also upregulated by
522 PRAMEL7 overexpression (Figure 5L), suggesting that PRAMEL7 controls genetic
523 program for 2CLCs through the upregulation of *Dux* expression in ESCs. Next, we
524 focused on cluster 2, in which the genes were downregulated by *Dux* KO and this
525 downregulation was diminished by PRAMEL7 overexpression (Figure 5I). Cluster 2
526 was subdivided into two groups based on the gene expression dynamics in early mouse
527 development (Figure 5M). The first groups, clusters 2a and b, contained the maternal
528 factor, including *Dazl*, *Zp3,* and *Mael*. The second group consisted of clusters 2c-f, in
529 which genes were upregulated after major ZGA, including *Prameef17*, *Zp600* and *Sox17*.

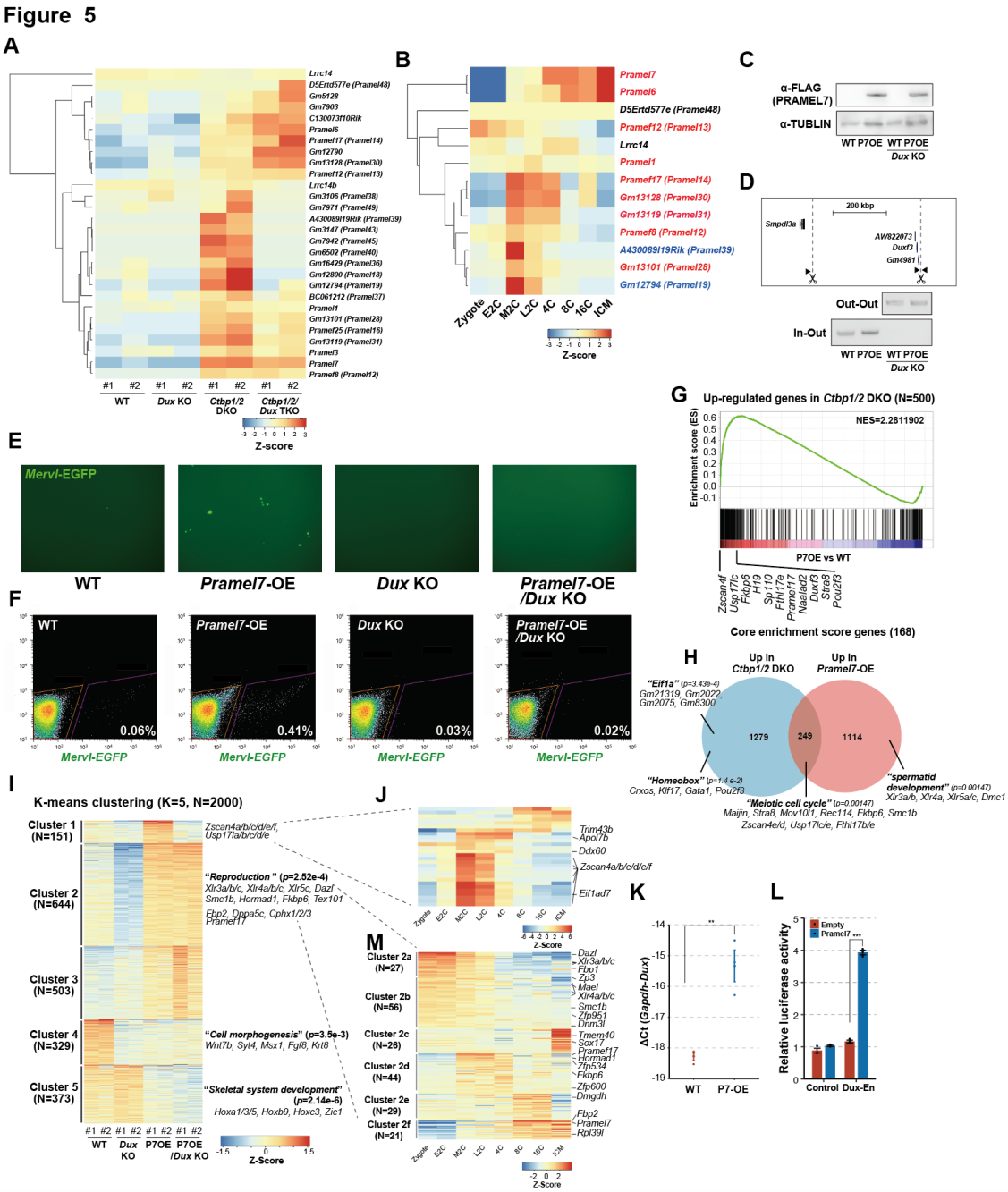


530

531 **Figure 5. PRMAEL7 controls two genetic cascades for ZGA.**

532 (A) The heatmap showing the hierarchical clustering of the expressions of Preme family
533 genes using RNA-Seq data in WT, *Dux* KO, *Ctbp1/2* DKO and *Ctbp1/2*/*Dux* KO ESCs.
534 (B) The heatmap shows the hierarchical clustering of the expressions of Preme family
535 genes using public single-cell RNA-Seq data in early mouse embryos (Gerlinger et al.,
536 2014). (C) Western blotting anti-FLAG (FLAG-PRAMEL) antibody using lysates of WT,
537 PRAMEL7-overexpressing, *Dux* KO and PRAMEL7-overexpressing *Dux* KO ESCs. (D)

538 Genotype PCR using the primer sets located outside the gRNA location to confirm the
539 large deletion of the *Dux* cluster. (E) Dark fields image visualizing *Mervl*-EGFP signals
540 in WT, PRAMEL7-overexpressing, *Dux* KO and PRAMEL7-overexpressing *Dux* KO
541 ESCs. (F) FACS analysis measuring the percentage of *Mervl*-EGFP-positive cells in WT,
542 PRAMEL7-overexpressing, *Dux* KO and PRAMEL7-overexpressing *Dux* KO ESCs. (G)
543 Gene set enrichment analysis (GSEA) using the upregulated genes by the *Ctbp1/2*
544 disruption to compare the gene expression of PRMAEL7-overexpressing ESCs with WT
545 ESCs. (H) Venn diagram showing the overlapping of the upregulated genes by the
546 *Ctbp1/2* disruption in ESCs with the upregulated genes by PRAMEL7 overexpression in
547 ESCs. (I) K-means clustering (K=5) of the gene expression in WT, PRAMEL7-
548 overexpressing, *Dux* KO, and PRAMEL7-overexpressing *Dux* KO ESCs using top 2000
549 differentially expressed genes. (J and M) K-means clustering analysis of the genes of
550 Cluster 1 and Cluster 4 using published single-cell RNA-Seq data of early mouse
551 embryo(Gerlinger et al., 2014) (K) RT-qPCR analysis of *Dux* in WT and PRAMEL7-
552 overexpressing ESCs. ΔCt value was calculated by subtracting the Ct value of *Dux* from
553 that of *Gapdh*. The means of ΔCt was calculated from three biological triplicates. ***$P$
554 $< 0.001$, **$P < 0.005$, *$P < 0.05$ (Tukey-Kramer multiple comparison test). (L) The effect
555 of PRAMEL7 overexpression against luciferase activity regulated by the *Dux* enhancer
556 region. Relative luciferase activity was calculated by setting the luciferase activity of the
557 empty vector as 1. The means of relative luciferase activity was calculated from three
558 biological triplicates. ***$P < 0.001$, **$P < 0.005$, *$P < 0.05$ (Tukey-Kramer multiple
559 comparison test).

560

561 ***Dux controls a part of genetic cascades for the ZGA program through the PRAMEL7***
562 ***functions***

563 We generated *Pramel7* KO ESCs and compared the gene expression profiles of WT,
564 *Pramel7* KO, *Dux* KO, *Pramel7*-OE and *Pramel7*-OE/*Dux* KO ESCs (Supplementary
565 Figure 1D). Hierarchical clustering analysis showed that *Dux* KO ESCs and *Pramel7*
566 KO ESCs were in the same cluster (Figure 6A). To investigate the similarity of global

567 gene expression between *Dux* KO ESCs and *Pramel7* KO ESCs, we employed scatter
568 plot analysis to visualize the relative expression alteration induced by *Dux* KO and
569 *Pramel7* KO (Figure 6B). The alterations in global expression observed in *Dux* KO and
570 *Pramel7* exhibited a positive correlation, particularly for downregulated genes. GSEA
571 also supported a positive correlation of expression changes between *Dux* KO and
572 *Pramel7* KO (Figure 6C, D). The Venn diagram using the upregulated or
573 downregulated genes by *Dux* KO and *Pramel7* KO showed the shared genes and
574 independent genes regulated by DUX and PRAMEL7 (Figure 6E, F). The genes
575 associated with ZGA were separated into DUX-dependent (*Zscan4* family) and
576 DUX/PRAMEL7-dependent (*Cphx* and *Zfp534/600*). Since we found that the
577 expression of *Pramel7* was found to be significantly reduced in *Dux* KO ESCs (Figure
578 6G), we tested the possibility that PRAMEL7-overexpression could rescue the
579 phenotype of *Dux* KO ESCs. The alteration of global gene expression by *Dux* KO in
580 WT ESCs and PRAMEL7 overexpression in *Dux* KO ESCs demonstrated a negative
581 correlation (Figure 6H). Furthermore, GSEA demonstrated that the overexpression of
582 PRAMEL7 in *Dux* KO ESCs effectively rescued the downregulated genes resulting
583 from *Dux* KO (Figure 6I). These findings indicate that DUX controls two genetic
584 pathways of the 2C program; one is directly regulated by DUX, and the other is
585 regulated by activation.

**Figure 6**

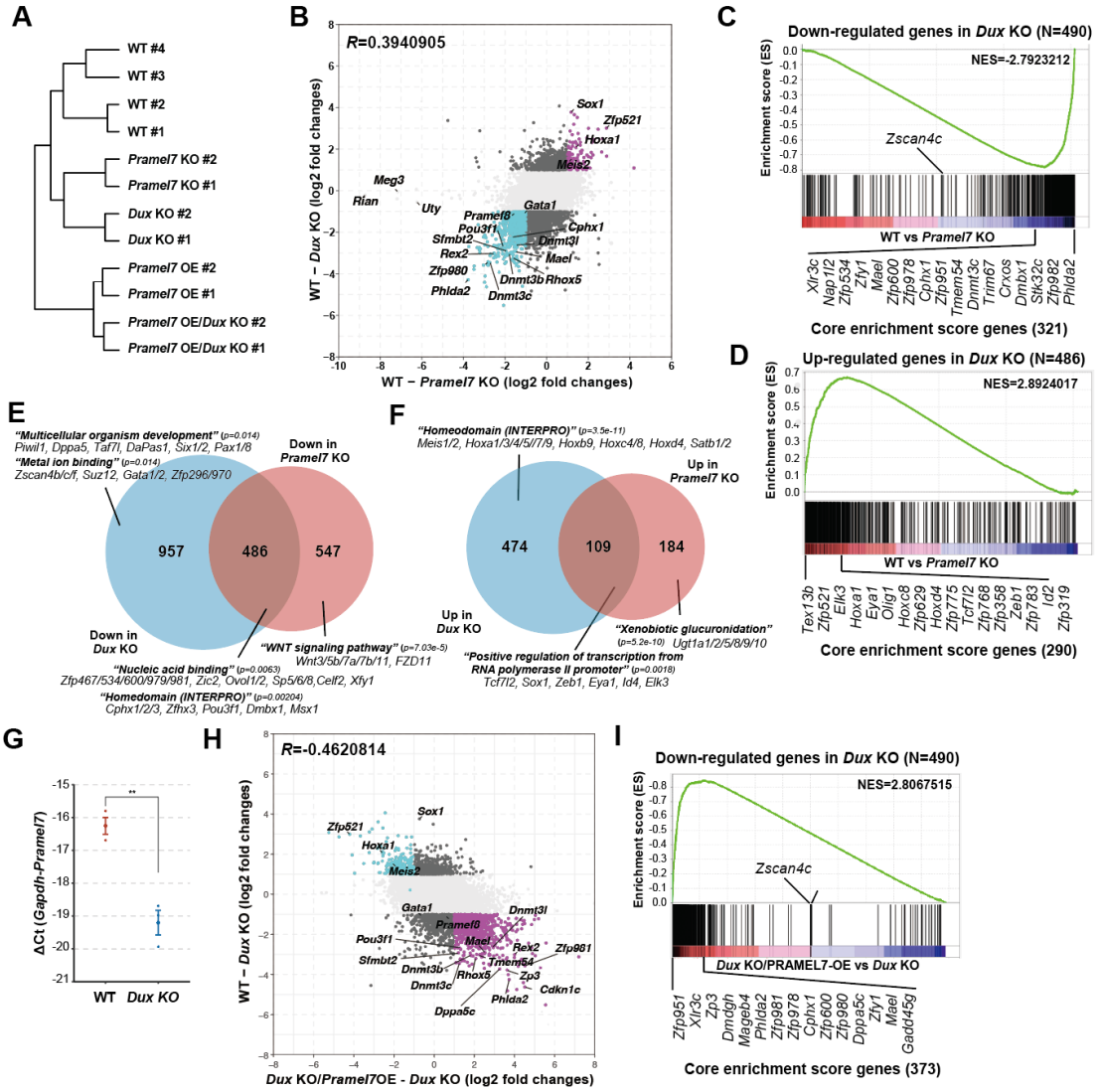


586

587 **Figure 6. DUX regulates parts of the genetic program for ZGA by activating**

588 ***Pramel7*.**

589 (A) Hierarchical clustering analysis of WT ESCs, *Pramel7* KO ESCs, *Dux* KO ESCs,
590 PRMAEL7-overexpressing ESCs and PRMAEL7-overexpressing *Dux* KO ESCs based
591 on the gene expression. (B) Scatter plot analysis of the correlation between the expression
592 changes by *Dux* KO and *Pramel7* KO in WT ESCs. (C) Gene set enrichment analysis
593 (GSEA) using the down-regulated genes by the *Dux* KO to compare the gene expression
594 of *Pramel7* KO ESCs with WT ESCs. (D) Gene set enrichment analysis (GSEA) using
595 the upregulated genes by the *Dux* KO to compare the gene expression of *Pramel7* KO
596 ESCs with WT ESCs. (E) Venn diagram showing the overlapping of the down-regulated

genes by *Dux* KO in ESCs with the down-regulated genes by *Pramel7* KO in ESCs. (F) Venn diagram showing the overlapping of the upregulated genes by *Dux* KO in ESCs with the upregulated genes by *Pramel7* KO in ESCs. (G) qRT-PCR analysis of *Pramel7* in wild type and *Dux* KO ESCs. ΔCt value was calculated by subtracting the Ct value of *Pramel7* from that of *Gapdh*. The means of ΔCt was calculated from three biological triplicates. ***$P < 0.001$, **$P < 0.005$, *$P < 0.05$ (Tukey-Kramer multiple comparison test). (H) Scatter plot analysis of the correlation between the expression changes by *Dux* KO in WT ESCs and *Pramel7*-OE in *Dux* KO ESCs. (K) Gene set enrichment analysis (GSEA) using the down-regulated genes by the *Dux* KO to compare the gene expression of PRMAEL7-overexpressing in *Dux* KO ESCs with *Dux* KO ESCs.

609 **Discussion**

**Figure 7**

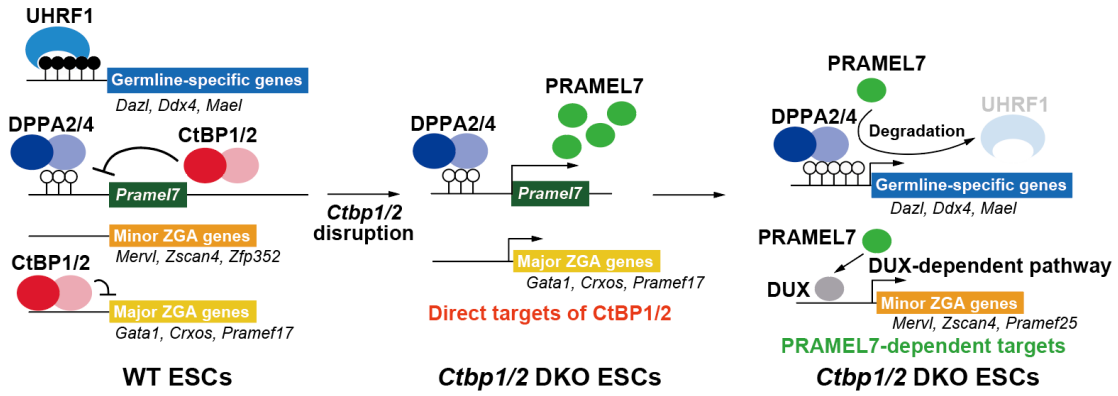


610

611 **Figure 7. A schematic model for the activation of 2C-related genes by the Ctbp1/2**

612 **disruption.**

613 In wild-type embryonic stem cells (ESCs), minor and major ZGA genes and germline-

614 specific genes are repressed. *Pramel7* and some parts of major ZGA genes are rapidly

615 reactivated following the disruption of *Ctbp1/2*. PRAMEL7 activates germline-specific

616 genes and minor ZGA genes in a manner dependent on UHRF1 degradation or DUX,

617 respectively.

618

619 In this study, we revealed that the disruption of *Ctbp1/2* in ESCs activates DUX-

620 dependent and independent molecular cascades to establish totipotent states (Figure 7).

621 Most DUX-dependent genes activated by *Ctbp1/2* DKO are transiently expressed at

622 around 2C stage embryo, belonging to the minor ZGA genes. In contrast, DUX-

623 independent genes activated by *Ctbp1/2* DKO are categorized into two groups:

624 Maternally expressed genes and the genes upregulated after major ZGA, some of which

625 are regulated by DPPA2. PRAMEL7, which is directly activated by the disruption of

626 *Ctbp1/2* in a DUX-independent manner, controls DUX-dependent genetic cascades
627 through DUX activation and DUX-independent genetic cascades. We present new
628 insights into the DUX-independent molecular pathways that ensure the early mouse
629 embryo's survival.
630 Our data clearly showed that reducing CtBP protein levels in ESCs activates a part of the
631 genetic program regulating the development of early mouse embryos. scRNA-seq data of
632 early mouse embryos shows that a large amount of *Ctbp2* mRNA is maternally deposited
633 in unfertilized eggs and significantly reduced after fertilization (Gerlinger et al., 2014).
634 In contrast, the protein level of CtBP2 was consistent between the 2CLCs that emerged
635 from pluripotent stem cells and pluripotent stem cells, indicating that the expression
636 levels of CtBP proteins are quite different between 2C embryos and 2CLCs. This
637 difference may explain the dependence of the emergence of 2CLCs and early mouse
638 development on DUX functions. However, the molecular mechanism of the clearance of
639 *Ctbp2* mRNA after fertilization is currently unclear. It has been reported that the inhibition
640 of minor ZGA inhibition with 5, 6-dichloro-1-β-D-ribofuranosyl-benzimidazole (DRB)
641 failed in a part of maternal mRNA clearance, including maternal *Ctbp2* mRNA (Abe et
642 al., 2018). Moreover, the maternal knockout of B-cell translocation gene-4 (BTG4),
643 which involves the maternal mRNA clearance by CCR4-NOT-dependent deadenylation,
644 was found to impair the maternal *Ctbp2* mRNA clearance. (Yu et al., 2016). These
645 findings suggest that the products of minor ZGA may work with BTG4 to destabilize the
646 clearance of maternal *Ctbp2* mRNA.
647

648 Transcriptome analysis of several knockout lines of ESCs provided evidence that the
649 activated genes by the disruption of *Ctbp1/2* are subdivided into three groups: both DUX
650 and DPPA2-dependent genes, DPPA2-dependent genes and both DUX and DPPA2-
651 independent genes (Figure 7). DUX- and DPPA2-dependent genes were enriched in the
652 minor ZGA genes at 2C embryo, including the *Zscan4* family. In contrast, DUX and
653 DPPA2-independent genes contained maternal factors, including *Dazl* and *Mael*, and the
654 major ZGA genes (*Gata1*, *Crxos* and *Pramef17*) in the early mouse embryo. A previous
655 study has shown that totipotent-like stem cells (TLSCs) induced by the chemical
656 inhibitors of DOT1L, KDM5B and G9a/GLP expressed a large number of minor and
657 major ZGA genes as well as maternal genes (Yang et al., 2022). The re-establishment of
658 broad H3K4me3 domains induced by the inhibition of KDM5B is thought to be involved
659 in the upregulation of maternal genes. However, because TLSCs were not established
660 using *Dux* KO ESCs, the role of DUX in the transition from ESCs to TLSCs and the
661 upregulation of maternal genes are largely unknown. Our data demonstrate that the
662 upregulation of maternal genes by *Ctbp1/2* DKO does not depend on DUX function and
663 is partially regulated by *Pramel7* induction.
664
665 *Prame* is one of the most amplified gene families in mammals, and the mouse *Prame*
666 gene family is the third largest family in the genome (Chang et al., 2011). We presented
667 that the disruption of *Ctbp1/2* activates the majority of *Prame* family genes in ESCs, some
668 of which are upregulated by DUX function and the rest directly by CtBP1/2. Interestingly,
669 *Prame* genes that depend on DUX are enriched in minor ZGA genes, including *Zscan4*

670 family genes, while *Prame* genes independent of DUX are upregulated after major ZGA.
671 Many *Prame* genes are repressed soon after induction of CtBP2 in *Ctbp1/2* DKO ESCs,
672 indicating that CtBP1/2 directly repress *Prame* family genes in ESCs. However, the
673 positive regulators of *Prame* family genes are largely unknown. Recent reports revealed
674 that the overexpression of multiple homeobox genes, oocyte-specific homeobox (Obox)
675 activate minor and major ZGA genes in mESCs (Guo et al., 2024; Ji et al., 2023;
676 Sakamoto et al., 2024). Interestingly, the overexpression of OBOX3/5 but not DUX
677 activate *Prame7* and *Pramef17* (*Pramel14*), which are upregulated by the loss of *Ctbp1/2*
678 without DUX, but not *Gm12794* (*Pramel19*) and *A430089l19Rik* (*Pramel39*), which are
679 upregulated in a DUX-dependent manner (Sakamoto et al., 2024). Because Obox family
680 genes were silent in *Ctbp1/2* DKO ESCs, another positive regulator for Prame family
681 genes may be activated by *Ctbp1/2* DKO in mESCs. Expression of *Prame* family genes
682 has been discovered in various cancer and germline cells (Kern et al., 2021), and the
683 expression pattern of *Prame* family genes is similar to that of *Pou5f1* (Oct4) (Bortvin et
684 al., 2003), suggesting that transcriptional network centred upon OCT4 is a positive
685 regulator of *Prame* family genes.
686
687 Although DUX is a master regulator for the transition from pluripotent stem cells into
688 2CLC, *Dux* KO embryos are normally born and fertile. The data presented here show that
689 most of the *Dux* KO phenotype is rescued by PRAMEL7 overexpression in ESCs. It has
690 been reported that *Prame* family genes are upregulated from the early phase of 2CLCs
691 emergence traced by the *Zscan4* and *Mervl* reporter system based on the scRNA-seq

692 (Eckersley-Maslin et al., 2016; Rodriguez-Terrones et al., 2018) and MERVL-positive
693 2CLCs are eliminated by *Dux* KO (De Iaco et al., 2017). Based on these findings, we
694 speculate that DUX controls two major genetic cascades for the development of early
695 mouse embryos: direct transcriptional regulation and PRAME-mediated transcriptional
696 regulation. *Dux* KO ESCs showed a significant reduction of *Pramel7* transcription, while
697 the expression of *Pramel7* is normally activated in *Dux* KO embryos at the mid-2-cell
698 stage (Guo et al., 2019). These findings suggest that the DUX-independent mechanism
699 activates the *Prame* family *in vivo*, and this mechanism might be induced in ESCs by the
700 disruption of *Ctbp1/2*.
701
702 Our results provide new insights into understanding DUX-independent genetic cascades,
703 ensuring the development of early mouse embryos. Although the visualization of 2CLCs
704 marked by the transcription of MERVL contributed to identifying the regulators for the
705 transition between pluripotent stem cells and 2CLCs, the knockout phenotypes of the
706 identified factors were functionally dependent on DUX. Developing the visualization
707 system for new 2CLCs regulating by DUX-independent genetic cascades in ESCs will be
708 needed.
709
710

## References


**Abe, K., Funaya, S., Tsukioka, D., Kawamura, M., Suzuki, Y., Suzuki, M. G., Schultz, R. M. and Aoki, F.** (2018). Minor zygotic gene activation is essential for mouse preimplantation development. *Proceedings of the National Academy of Sciences* **115**, E6780–E6788.

**Bortvin, A., Eggan, K., Skaletsky, H., Akutsu, H., Berry, D. L., Yanagimachi, R., Page, D. C. and Jaenisch, R.** (2003). Incomplete reactivation of Oct4-related genes in mouse embryos cloned from somatic nuclei. *Development* **130**, 1673–1680.

**Chang, T. C., Yang, Y., Yasue, H., Bharti, A. K., Retzel, E. F. and Liu, W. S.** (2011). The expansion of the PRAME gene family in Eutheria. *PLoS One* **6**,.

**Chen, Z. and Zhang, Y.** (2019). Loss of DUX causes minor defects in zygotic genome activation and is compatible with mouse development. *Nat Genet* **51**, 947–951.

**De Iaco, A., Planet, E., Coluccio, A., Verp, S., Duc, J. and Trono, D.** (2017). DUX-family transcription factors regulate zygotic genome activation in placental mammals. *Nat Genet* **49**, 941–945.

**Eckersley-Maslin, M. A., Svensson, V., Krueger, C., Stubbs, T. M., Giehr, P., Krueger, F., Miragaia, R. J., Kyriakopoulos, C., Berrens, R. V., Milagre, I., et al.** (2016). MERVL/Zscan4 Network Activation Results in Transient Genome-wide DNA Demethylation of mESCs. *Cell Rep* **17**, 179–192.

**Eckersley-maslin, M. A., Alda-catalinas, C. and Reik, W.** (2018). Dynamics of the epigenetic landscape during the maternal- to-zygotic transition. *Nat Rev Mol Cell Biol* **19**, 436–450.

**Eckersley-Maslin, M., Alda-Catalinas, C., Blotenburg, M., Kreibich, E., Krueger, C. and Reik, W.** (2019). Dppa2 and Dppa4 directly regulate the Dux-driven zygotic transcriptional program. *Genes Dev* **33**, 194–208.

**Eckersley-maslin, M. A., Parry, A., Blotenburg, M., Krueger, C., Ito, Y., Nila, V., Franklin, R., Narita, M., Santos, C. S. D. and Reik, W.** (2020). Epigenetic priming by Dppa2 and 4 in pluripotency facilitates multi-lineage commitment. *Nat Struct Mol Biol* **27**, 696–705.

**Engelen, E., Brandsma, J. H., Moen, M. J., Signorile, L., Dekkers, D. H. W., Demmers, J., Kockx, C. E. M., Ozgür, Z., Van Ijcken, W. F. J., Van Den Berg, D. L. C., et al.** (2015). Proteins that bind regulatory regions identified by histone

743 modification chromatin immunoprecipitations and mass spectrometry. *Nat Commun*
744 **6**,.
745 **Ge, S. X., Son, E. W. and Yao, R.** (2018). iDEP: An integrated web application for
746 differential expression and pathway analysis of RNA-Seq data. *BMC Bioinformatics*
747 **19**, 1–24.
748 **Gerlinger, M., Swanton, C., Greaves, M. and Maley, C. C.** (2014). Single-Cell RNA-
749 Seq Reveals Dynamic, Random Monoallelic Gene Expression in Mammalian Cells.
750 **343**, 193–196.
751 **Graf, U., Casanova, E. A., Wyck, S., Dalcher, D., Gatti, M., Vollenweider, E.,**
752 **Okoniewski, M. J., Weber, F. A., Patel, S. S., Schmid, M. W., et al.** (2017).
753 Pramel7 mediates ground-state pluripotency through proteasomal-epigenetic
754 combined pathways. *Nat Cell Biol* **19**, 763–773.
755 **Gretarsson, K. H. and Hackett, J. A.** (2020). Dppa2 and Dppa4 counteract de novo
756 methylation to establish a permissive epigenome for development. *Nat Struct Mol*
757 *Biol* **27**, 706–716.
758 **Grow, E. J., Weaver, B. D., Smith, C. M., Guo, J., Stein, P., Shadle, S. C.,**
759 **Hendrickson, P. G., Johnson, N. E., Butterfield, R. J., Menafra, R., et al.** (2021).
760 p53 convergently activates Dux/DUX4 in embryonic stem cells and in
761 facioscapulohumeral muscular dystrophy cell models. *Nat Genet* **53**, 1207–1220.
762 **Guo, M., Zhang, Y., Zhou, J., Bi, Y., Xu, J., Xu, C., Kou, X., Zhao, Y., Li, Y., Tu, Z.,**
763 **et al.** (2019). Precise temporal regulation of Dux is important for embryo
764 development. *Cell Res* **7**, 1–4.
765 **Guo, Y., Kitano, T., Inoue, K., Murano, K., Hirose, M., Li, T. D., Sakashita, A., Ishizu,**
766 **H., Ogonuki, N., Matoba, S., et al.** (2024). Obox4 promotes zygotic genome
767 activation upon loss of dux. *Elife* **13**, 1–25.
768 **Hendrickson, P. G., Doráis, J. A., Grow, E. J., Whiddon, J. L., Lim, J.-W., Wike, C.**
769 **L., Weaver, B. D., Pflueger, C., Emery, B. R., Wilcox, A. L., et al.** (2017).
770 Conserved roles of mouse DUX and human DUX4 in activating cleavage-stage
771 genes and MERVL/HERVL retrotransposons. *Nat Genet* **49**, 925–934.
772 **Hu, Z., Tan, D. E. K., Chia, G., Tan, H., Leong, H. F., Chen, B. J., Lau, M. S., Tan,**
773 **K. Y. S., Bi, X., Yang, D., et al.** (2020). Maternal factor NELFA drives a 2C-like
774 state in mouse embryonic stem cells. *Nat Cell Biol* **22**, 175–186.
775 **Hulsen, T., de Vlieg, J. and Alkema, W.** (2008). BioVenn - A web application for the

776 comparison and visualization of biological lists using area-proportional Venn
777 diagrams. *BMC Genomics* **9**, 1–6.
778 **Ishiuchi, T., Enriquez-Gasca, R., Mizutani, E., Bošković, A., Ziegler-Birling, C.,**
779 **Rodriguez-Terrones, D., Wakayama, T., Vaquerizas, J. M. and Torres-Padilla,**
780 **M.-E.** (2015a). Early embryonic-like cells are induced by downregulating
781 replication-dependent chromatin assembly. *Nat Struct Mol Biol* **22**, 662–71.
782 **Ishiuchi, T., Enriquez-gasca, R., Mizutani, E., Bošković, A., Ziegler-birling, C.,**
783 **Rodriguez-terrones, D., Wakayama, T. and Vaquerizas, J. M.** (2015b). Articles
784 Early embryonic-like cells are induced by downregulating replication-dependent
785 chromatin assembly. *Nature Publishing Group* **22**, 662–671.
786 **Ji, S., Chen, F., Stein, P., Wang, J., Zhou, Z., Wang, L., Zhao, Q., Lin, Z., Liu, B., Xu,**
787 **K., et al.** (2023). OBOX regulates mouse zygotic genome activation and early
788 development. *Nature* **620**, 1047–1053.
789 **Kern, C. H., Yang, M. and Liu, W. S.** (2021). The PRAME family of cancer testis
790 antigens is essential for germline development and gametogenesis. *Biol Reprod* **105**,
791 290–304.
792 **Kim, T. W., Kang, B. H., Jang, H., Kwak, S., Shin, J., Kim, H., Lee, S. E., Lee, S. M.,**
793 **Lee, J. H., Kim, J. H., et al.** (2015). Ctbp2 Modulates NuRD-Mediated
794 Deacetylation of H3K27 and Facilitates PRC2-Mediated H3K27me3 in Active
795 Embryonic Stem Cell Genes during Exit from Pluripotency. *Stem Cells* **33**, 2442–
796 2455.
797 **Kreibich, E., Blotenburg, M., Alda-Catalinas, C., Reik, W., Krueger, C. and**
798 **Eckersley-Maslin, M.** (2019). Dppa2 and Dppa4 directly regulate the Dux-driven
799 zygotic transcriptional program. *Genes Dev* **33**, 194–208.
800 **Macfarlan, T. S., Gifford, W. D., Driscoll, S., Lettieri, K., Rowe, H. M., Bonanomi,**
801 **D., Firth, A., Singer, O., Trono, D. and Pfaff, S. L.** (2012). Embryonic stem cell
802 potency fluctuates with endogenous retrovirus activity. *Nature* **487**, 57–63.
803 **Percharde, M., Lin, C., Yin, Y., Huang, B., Shen, X., Ramalho-santos, M., Percharde,**
804 **M., Lin, C., Yin, Y., Guan, J., et al.** (2018). Article A LINE1-Nucleolin Partnership
805 Regulates Early Development and ESC Identity Article A LINE1-Nucleolin
806 Partnership Regulates Early Development and ESC Identity. *Cell* **174**, 1–15.
807 **Robinson, J. T., Thorvaldsdóttir, H., Winckler, W., Guttman, M., Lander, E. S., Getz,**
808 **G. and Mesirov, J. P.** (2011). Integrative genomics viewer. *Nat Biotechnol* **29**, 24–

26.

**Rodriguez-Terrones, D., Gaume, X., Ishiuchi, T., Weiss, A., Kopp, A., Kruse, K., Penning, A., Vaquerizas, J. M., Brino, L. and Torres-Padilla, M. E.** (2018). A molecular roadmap for the emergence of early-embryonic-like cells in culture. *Nat Genet* **50**, 106–119.

**Sakamoto, M., Ito, A., Wakayama, S., Sasaki, H., Wakayama, T. and Ishiuchi, T.** (2024). Detection of newly synthesized RNA reveals transcriptional reprogramming during ZGA and a role of Obox3 in totipotency acquisition. *Cell Rep* **43**, 114118.

**Whiddon, J. L., Langford, A. T., Wong, C. J., Zhong, J. W. and Tapscott, S. J.** (2017). Conservation and innovation in the DUX4-family gene network. *Nat Genet* **49**, 935–940.

**Wolf, G., de Iaco, A., Sun, M. A., Bruno, M., Tinkham, M., Hoang, D., Mitra, A., Ralls, S., Trono, D. and Macfarlan, T. S.** (2020). Krab-zinc finger protein gene expansion in response to active retrotransposons in the murine lineage. *Elife* **9**, 1–22.

**Wu, K., Liu, H., Wang, Y., He, J., Xu, S., Chen, Y., Kuang, J., Liu, J., Guo, L., Li, D., et al.** (2020). SETDB1-Mediated Cell Fate Transition between 2C-Like and Pluripotent States. *Cell Rep* **30**, 25-36.e6.

**Yamamoto, M., Suwa, Y., Sugiyama, K., Okashita, N., Kawaguchi, M., Tani, N., Matsubara, K., Nakamura, A. and Seki, Y.** (2020). PRDM14-CtBP1/2-PRC2 complex regulates transcriptional repression during transition from primed to naïve pluripotency. *J Cell Sci* **133**, 1–13.

**Yang, M., Yu, H., Yu, X., Liang, S., Hu, Y., Luo, Y., Izsvák, Z., Sun, C. and Wang, J.** (2022). Chemical-induced chromatin remodeling reprograms mouse ESCs to totipotent-like stem cells. *Cell Stem Cell* **29**, 400-418.e13.

**Yu, C., Ji, S. Y., Sha, Q. Q., Dang, Y., Zhou, J. J., Zhang, Y. L., Liu, Y., Wang, Z. W., Hu, B., Sun, Q. Y., et al.** (2016). BTG4 is a meiotic cell cycle-coupled maternal-zygotic-transition licensing factor in oocytes. *Nat Struct Mol Biol* **23**, 387–394.

**Zhang, T., Zhang, Z., Dong, Q., Xiong, J. and Zhu, B.** (2020). Histone H3K27 acetylation is dispensable for enhancer activity in mouse embryonic stem cells. *Genome Biol* **21**, 1–7.

842 **Author Contributions**

843 Y.S. conceived the study and experimental design, performed experiments and wrote the
844 manuscript. K.S., K.Y. and N.H. performed most experiments. R.M. M.M., A.S. and Y.M
845 performed some experiments. K.S., K.Y. and N.H. contributed equally to this work.

846

847 **Acknowledgements**

848 We thank all members of Seki laboratory for stimulating discussions. This study was
849 supported by JSPS KAKENHI Grant Numbers JP18H02422, JP20H05375 and
850 JP22H04682.

851

852 **Conflict of interest**

853 The authors declare no competing interests.

854

855 **Data availability**

856 RNA-Seq data has been deposited in Gene Expression Omnibus (GSE253944)

857

858

859

860